Electrostatic Control of the Tryptophan Radical in Cytochrome *c* Peroxidase[†,‡]

Tiffany P. Barrows,[§,#] B. Bhaskar,[§,#] and Thomas L. Poulos*[,§,||,⊥,#]

Departments of Molecular Biology and Biochemistry, Physiology and Biophysics, and Chemistry and Program in Macromolecular Structure, University of California, Irvine, California 92697

Received March 9, 2004; Revised Manuscript Received April 30, 2004

ABSTRACT: Previously a K^+-binding site, analogous to that found in ascorbate peroxidase (APX), was engineered into cytochrome *c* peroxidase (CcP) to test the hypothesis that the bound K^+ influences the stability of the Trp191 cation radical formed during the CcP catalytic cycle (Bonagura et al., (1996) *Biochemistry 35*, 6107 and Bonagura et al., (1999) *Biochemistry 38*, 5528). Characterization of this mutant, designated CcPK2, showed that the stability of the Trp191 cation radical is dependent on the occupancy of the engineered K^+ site and that the Trp191 radical was much less stable in this mutant than in wild-type CcP. The mutations Met230Leu, Met231Gln, and Met172Ser have now been constructed on the CcPK2 mutant template to test if the Met residues also contribute to the stabilization of the Trp191 cation radical. Crystal structures show that the mutations affect only the local structure near the sites of mutation. Removal of these electronegative residues located less than 8 Å from the Trp radical results in a further destabilization of the Trp radical. The characteristic EPR signal associated with the Trp radical is significantly narrowed and is characteristic of a tyrosine radical signal. Double-mixing stopped-flow experiments, where the delay time between the formation of CcP compound **I** and its mixing with horse heart ferrocytochrome *c* is varied, show that the stability of the Trp radical decreases as the Met residues are removed from the proximal cavity. When taken together, these results demonstrate a strong correlation between the experimentally determined stability of the Trp191 radical, the enzyme activity, and the calculated electrostatic stabilization of the Trp191 radical.

Amino acid centered free radicals are critically important in a number of enzymes, which include ribonucleotide reductase, pyruvate formate lyase, prostaglandin H synthase, galactose oxidase, and DNA photolyase (*1*). Yeast cytochrome *c* peroxidase (CcP)[1] is also included in this list because CcP forms a stable tryptophan radical during its normal catalytic cycle (*2*, *3*). Owing to the stability of the CcP Trp radical and the ability to generate CcP mutants and mutant crystal structures, CcP has proven to be an ideal enzyme for unraveling the details of how redox enzymes store and stabilize oxidizing equivalents.

Like CcP, most well-studied nonmammalian heme peroxidases are single polypeptide chains on the order of 30−40 kD and contain a single noncovalently bound heme. Typical of all heme peroxidases, CcP reduces one molecule of H_2O_2 to two molecules of water through the oxidation of two molecules of substrate.

$$Fe^{3+}\,R + H_2O_2 \rightarrow \underset{\text{compound } \mathbf{I}}{Fe^{4+}{-}O\,R^{\bullet+}} + H_2O \quad (1)$$

$$Fe^{4+}{-}O\,R^{\bullet+} + \text{substrate} \rightarrow \underset{\text{compound } \mathbf{II}}{Fe^{4+}{-}O\,R} + \text{oxidized substrate} \quad (2)$$

$$Fe^{4+}{-}O\,R + \text{substrate} \rightarrow \underset{\text{resting state}}{Fe^{3+}\,R} + \text{oxidized substrate} + H_2O \quad (3)$$

In the first step of the reaction, H_2O_2 oxidizes the iron and an organic moiety, R, to give compound **I**. Compound **I** is then reduced by the substrate in two successive one electron-transfer reactions to regenerate the resting enzyme. In most heme peroxidases, $R^{\bullet+}$ is a porphyrin-π cation radical (*4*). In CcP, however, $R^{\bullet+}$ is the Trp191 cation radical (*2*).

Precisely why CcP forms a Trp radical, while other peroxidases form a porphyrin radical, has been a topic of considerable interest (*5*−*8*). Before structural studies on ascorbate peroxidase (APX) were carried out, this difference was attributed to the presence of a Trp residue in the proximal heme pocket of CcP, while most other heme peroxidases have a Phe at this position. When the APX sequence became available, it was clear that Trp179 in APX is homologous to Trp191 in CcP (*9*), the site of radical formation. When the APX X-ray structure was solved, it showed that Trp179 in APX is positioned in the active site analogous to Trp191

[†] This work was supported by NIH Grant GM42614.

[‡] PDB coordinates and structure factors have been deposited in the Protein Data Bank under accession numbers 1SOG and 1STQ.

* To whom correspondence should be addressed. Phone: (949) 824-7020. Fax: (949) 824-3280. E-mail: poulos@uci.edu.

[§] Department of Molecular Biology and Biochemistry.

[||] Department of Physiology and Biophysics.

[⊥] Department of Chemistry.

[#] Program in Macromolecular Structure.

[1] Abbreviations: CcP, cytochrome *c* peroxidase; CcPK2, CcPK2M2, and CcPK2M3, mutants of CcP; APX, ascorbate peroxidase; EPR, electron paramagnetic resonance; ABTS, 2,2-azino-bis(3-ethylbenzthiazoline-6-sulfonate); IPTG, isopropyl-β-D-thiogalactopyranoside.

10.1021/bi049531g CCC: $27.50
Published on Web 06/15/2004

in CcP (*6*), and, like CcP, a conserved Asp hydrogen-bonds with both the proximal His heme ligand and Trp179. On the basis of such striking structural conservation, it was fully anticipated that APX would also form a Trp cation radical. However, freeze-quench EPR showed that, like other peroxidases, APX forms a porphyrin-π cation radical (*10*).

One obvious structural difference between CcP and APX that might determine whether the porphyrin or the Trp is oxidized is the K^+-binding site located about 8 Å from Trp179 in APX. CcP has a water at this location. It was reasoned that the presence of the positively charged K^+ might destabilize the positive charge on the Trp radical in APX compared to CcP, and hence, the porphyrin is preferentially oxidized in APX (*10*). Previous work from our laboratory has focused on the K^+-binding site in APX. By iterative protein engineering, Bonagura et al. (*7*) showed that the stability of the Trp191 radical in a CcP mutant designated CcPK2 could be decreased by the titration of potassium into an engineered metal-binding site homologous to the K^+-binding site of APX. These studies showed that the main contribution of the K^+ site is to destabilize the Trp191 cation radical but not to its initial formation. The Trp191 radical still forms in the K^+ mutants but its stability is greatly diminished. Electrostatic calculations also indicate that the engineered K^+ site is only partially responsible for the stability of the Trp191 radical (*11*). Using this mutant as a starting point, we have introduced further mutations in an effort to continue to probe what structural features stabilize the Trp191 radical. Because the sulfur of methionine is electronegative, the presence of three Met residues within 8 Å of the Trp radical in CcP may account for the difference in the radical location between APX and CcP. Indeed, previous work has implicated Met as important in controlling oxidizing equivalents in compound **I**. Liu et al. (*12*) showed that Met172 is essential for intramolecular electron transfer from the Trp191 radical to the $Fe^{4+}-O$ center, while Fishel et al. (*13*) found that Met230 and Met231 are important in controlling the line shape of the Trp191 EPR signal. To test the role that active-site Met residues might play in electrostatic stabilization of the Trp191 radical, Met230 and Met231 were mutated to Leu and Gln, the corresponding residues in APX. This protein is called CcPK2M2. Additionally, Met172 in the mutant CcPK2M2 was mutated to Ser, the equivalent residue in APX, yielding CcPK2M3. This paper describes the detailed structural, kinetic, and spectroscopic characterization of the mutant enzymes CcPK2M2 and CcPK2M3.

MATERIALS AND METHODS

Enzymes and reagents for site-directed mutagenesis were purchased from New England Biolabs Inc. (Beverly, MA), Invitrogen Corp (Carlsbad, CA), and Qiagen Inc. (Valencia, CA). Chromatography columns were purchased from Amersham-Pharmacia Biotechnologies (Uppsala, Sweden). Hydrogen peroxide 30% w/v was purchased from Sigma (St. Louis, MO). Cytochrome *c* (cyt *c*) was purchased from Sigma (St. Louis, MO) and was used in steady-state assays without further purification or analysis of isozyme content. 2-Methyl-pentanediol was purchased from Aldrich (St. Louis, MO). 2,2-Azino-bis(3-ethylbenzthiazoline-6-sulfonate) (ABTS) was purchased from Roche (Indianapolis, IN). All other chemicals were purchased from EM Science (Gibbstown, NJ).

Site-Directed Mutagenesis. The plasmid containing a mutated CcP gene, CcPK2M2, was obtained from Dr. Chris A. Bonagura. This plasmid contained the following mutations A176T, G192T, A194N, T199D, and E201S constructed on the wild-type CcP template, which make up the previously reported CcPK2 (*7*, *8*), as well as the additional mutations M230L and M231Q. The mutant was designed to more closely resemble the proximal cavity of APX than that of the CcPK2 mutant. The removal of the Met residues was expected to reduce the electrostatic stabilization of the Trp radical. In an effort to better approximate the proximal site architecture of APX, Met172 was also changed to Ser, the equivalent residue in APX. This alteration was intended to further destabilize the Trp radical in CcP compound **I** by removing the last remaining Met within 8 Å of Trp191. The oligonucleotide GCTCTTAGTGGAGCTCACAACCTGG and its reverse complement were purchased from Qiagen's Operon Technologies (Alameda, CA). On the basis of preliminary results Tyr236 was targeted for mutagenesis with the goal of eliminating a Tyr-like radical. The oligonucleotide GCTGCCCACGGATTTTTCTTTGATTCAGG and its reverse compliment were purchased from Qiagen's Operon Technologies (Alameda, CA) to mutate Tyr236 to Phe. Site-directed mutagenesis was carried out by overlap extension using PCR (*14*), with the outside primers "T7" TAATACGACTCACTATAGG and "Lac-80" CAGTCACGACGTTGTAAAAC, which were also purchased from Qiagen's Operon Technologies. Mutations were confirmed by restriction analysis and DNA sequencing at DBS sequencing facility at University of California, Davis. The resulting mutants were called CcPK2M3 and CcPK2M3 Y236F.

Protein Expression and Purification. Plasmids containing recombinant CcPK2M2, CcPK2M3, and CcPK2M3 Y236F were transformed into *Escherichia coli* BL21(DE3) cells and the transformants were grown in 6 L of terrific broth with vigorous shaking at 37 °C until the cultures reached an OD_{600} of 0.9. At this point, IPTG was added to a final concentration of 0.75 mM to induce protein production from the T7 promoter, and shaking was reduced to 80 rpm. Pure protein was prepared as previously described by Fishel et al. (*15*) with minor modifications. However, because these mutants formed an oily precipitate rather than a crystalline solid with dialysis against distilled water, the protein was stored at −80 °C in 50 mM potassium phosphate at pH 6.0 rather than as a crystalline suspension. The CcP concentration was determined spectrophometrically using an extinction coefficient of 96 mM^{-1} cm^{-1} at 408 nm.

Steady-State Activity Assays. All spectrophotometric assays were carried out on a Cary 3E UV−visible spectrophotometer. Steady-state activity was measured using the native substrate of CcP, yeast cyt *c*. The assays on the wild-type protein were performed using a final concentration of 25 pM enzyme, while the mutant proteins were assayed at a final concentration of 10 nM. Assays of both wild-type and mutant proteins were carried out with a final concentration of reduced cyt *c* of 25 μM. The concentrations of all of the proteins involved in these assays were determined using known extinction coefficients, 96 mM^{-1} cm^{-1} at 408 nm for CcP and 27.7 mM^{-1} cm^{-1} at 550 nm for reduced cyt *c*. The kinetic trials were carried out in ion-free Tris-phosphate (pH 6.0) at both 10 and 100 mM ionic strength. The oxidation

of ferrous cyt *c* was followed at room temperature at a wavelength of 550 nm for 30 s.

Assays were also performed using a small molecule substrate. The steady-state turnover of the small molecule ABTS by wild-type and mutant CcP was studied to verify that the mutant enzymes were still able to receive electrons from external donors. Reactions with ABTS were carried out by mixing 10 nM wild-type or mutant protein with 250 μM H_2O_2 and 10−500 μM ABTS in 50 mM potassium phosphate at pH 6.0, as outlined by Iffland et al. (*16*), except BSA was omitted from the reaction mixture. The reaction was measured at 414 nm, where the oxidation of ABTS by the various CcP mutants could be monitored by observing the appearance of the green color of oxidized ABTS.

Transient-State Kinetics. Examination of the transient kinetic traces accompanying the reaction of heme peroxidases with H_2O_2 allows one to detect the presence of a porphyrin-π cation radical, because the formation of the porphyrin radical leads to a distinct color change from brown/red to green. When observing the kinetic changes at wavelengths across the Soret region, the formation of a porphyrin radical is accompanied by a large decrease in absorbance. Such experiments were carried out for wild-type CcP, CcPK2M2, and CcPK2M3 as well as CcPW191G, which served as a positive control for porphyrin radical formation. These stopped-flow experiments were carried out on a Hi-Tech Scientific model SF-51 stopped-flow spectrophotometer with a 1-cm path length. The formation of compound **I** in the wild-type and the various mutants was studied using 2 μM protein and between 1 and 10 μM H_2O_2, in 50 mM potassium phosphate at pH 6.0 and 7 °C. The reactants were mixed in a total volume of 100 μL, and the change in absorbance at various wavelengths (primarily 421 nm but also 403, 408, and 414 nm) was followed for 0.5 s.

Double-Mix Delay Transient-State Kinetics. The stability of the Trp radical was examined in wild-type CcP, CcPK2 with an additional Asn195Pro mutation (*17*), CcPK2M2, CcPK2M3, and CcPK2M3 Y236F using a procedure based on work by Hahm et al. (*18*). Experiments were carried out on an Applied Photophysics Ltd. SX.18MV-R stopped-flow instrument equipped with the SQ.1 option for sequential mixing and a flow cell with a 1-cm path length. A total of 14.5 μM CcP was reacted with a stoichiometric amount of H_2O_2 in a total volume of 220 μL (Mix 1). This mixing resulted in the formation of 7.25 μM CcP compound **I**, which was then aged for varying amounts of time ranging between 20 ms and 2 min. Aged compound **I** was then mixed with 2.5 μM horse heart ferrocytochrome *c* in a total volume of 180 μL (Mix 2), giving a volume of 400 μL for the 2 drives. The precise concentration of the compound **I** Trp radical in mix 2 was dependent on the stability of the Trp radical in compound **I**. The 3:1 stoichiometry of CcP to ferrocytochrome *c* was maintained for the wild-type and all mutant reactions to ensure that the oxidizing equivalent in the reaction was entirely from the Trp radical, with no contribution from Fe^{4+} reduction (*18*). The reaction was carried out in 100 mM potassium phosphate at pH 7.0 to slow the intermolecular electron-transfer reaction enough so that it could be followed within the dead-time limits of the stopped flow. The oxidation of ferrocytochrome *c* was monitored at 416 nm, and measurements were taken at 434 nm as a control to confirm that Fe^{4+} was not being reduced in the course of the reaction with ferrocytochrome *c*. All experiments were performed at room temperature. The resulting data were then fit using TableCurve 2D (version 5.01.01) and analyzed using Igor Pro (version 3.14).

Electron Paramagnetic Resonance (EPR). EPR spectroscopy was carried out on a Bruker ESP300 EPR spectrometer equipped with an air-products LTR3 liquid-helium cryostat at 4.0 K in the laboratory of Dr. H. B. Gray at the California Institute of Technology, Pasadena, CA. To observe the radical in compound **I**, 150 μL of 300 μM wild-type or mutant CcP protein and an equal volume of 360 μM H_2O_2 were combined. When the solution was completely mixed, it was transferred to a quartz EPR tube and flash-frozen in an *n*-hexanes−N_2(l) slurry. This process took between 40 and 60 s. The EPR spectra were obtained as an average of 10 scans of the field using the following parameters: microwave frequency, 9.475 GHz; microwave power, 0.101 mW; modulation amplitude, 6 G; modulation frequency, 100 kHz; field sweep rate, 19.07 G/s; receiver gain, 1.0×10^4 for wild-type CcP and CcPK2M3 and 2.5×10^4 for CcPK2M2; and time constant, 1.280 ms. The reaction was carried out in both 5 mM potassium phosphate at pH 6.0 and 5 mM ion-free Tris-phosphate at pH 6.0, and the results were compared.

X-ray Crystallography. Crystals were grown using vapor diffusion in 9-well depression plates at 4 °C. Crystals of CcPK2M2 were grown in 25% 2-methyl-2,4-pentanediol (MPD) in 50 mM Tris-phosphate at pH 6.0 and 13.3 mM mix of 18crown6 and 15crown5 ethers, at a protein concentration of 400 μM CcPK2M2. This tray was setup in a sandwich box pre-equilibrated with 30% MPD. The drops were allowed to equilibrate for approximately 24 h before they were touch-seeded with crystalline material from wild-type CcP crystals. Crystals were then grown for 2 weeks.

The protocol for crystal growth was adjusted slightly in the case of CcPK2M3. Because the mutant protein would not crystallize by dialysis against water, only protein from the peak fraction off of the final column was used for crystallographic studies. Additionally, the crystal used for the X-ray experiments was grown with a lower initial precipitant concentration using only 15% MPD, in buffers containing 50 mM potassium phosphate at pH 6.0. Owing to the lower occupancy of the potassium site in the refined structure of CcPK2M2, the crown ethers were eliminated.

Crystals were flash-frozen in liquid nitrogen, and 135 frames of data were collected at one degree oscillations on an R-axis IV imaging plate and a Rigaku rotating anode X-ray source fitted with Osmic optics and equipped with a Crystal Logic cryogenic N_2 delivery system. The data were processed, indexed, and integrated using Denzo (version 1.9.1), and the integrated data were then scaled using Scalepack (version 1.9.0) (*19*). CcPK2 was used as the starting model for refinement in CNS (version 1.0) (*20*). Data collection and refinement statistics are shown in Table 1. The coordinates and structure factors have been deposited in the Protein Data Bank and have been assigned the PDB accession codes of 1SOG and 1STQ for CcPK2M2 and CcPK2M3, respectively.

Polaris Calculations. The energetic basis for the decrease in stability of the Trp191 radical was probed computationally with Polaris as implemented in the Molaris package (*21*). The Trp191 radical cation charges were obtained from Jensen

Table 1: Summary of Data Collection Statistics and Crystallographic Refinement

	CcPK2M2	CcPK2M3
Summary of Data Collection		
total number of reflections	373 716	493 346
number of unique reflections	46 421	42 860
completeness (%)	99.1	99.3
completeness in outer shell (%)	99.9	93.7
I/σ in the outer shell	28.89	13.85
space group	$P2_12_12_1$	$P2_12_12_1$
Refinement Statistics		
resolution	50−1.85	50−1.82
R_{factor} (%)	16.62	19.37
R_{free} (%)	20.13	21.69
rms deviation bonds (Å)	0.362	0.416
rms deviation bond angles	0.630	0.705
CA rmsd to wild-type CcP (Å)	0.160	0.154
CA rmsd to wild-type APX (Å)	0.965	0.969

et al. (*11*). Asp235, which accepts a hydrogen bond from Trp191, and Asp199, a K^+ ligand, were assigned a charge of −1, while K^+ was assigned a charge of +1. The remainder of the charges was the default settings of the program. Protein ligand−K^+ distances were constrained to the values found in the crystal structures using a force constant of 100 kcal/Å. The imidazole ring nitrogens of the heme ligand, His175, the indole nitrogen of Trp191, the side-chain oxygens of Asp235, and the iron atom were constrained to their crystallographic positions with a force constant of 150 kcal/Å. In this method, the electrostatic stability of the Trp191 cation was computed in water and compared to the stability in the protein. Although the resulting $\Delta\Delta G$ (movement from water to protein) was physically unreal, this provided a basis for comparing different proteins and mutants. The structure first was energetically relaxed for 1 ps to remove hot spots in the structure. $\Delta\Delta G$ was then computed over several configurations during a 40 ps molecular dynamics (MD) simulation. The key to this method is the Protein Dipoles Langevin Dipoles (PDLD) approach to modeling the solvent. Rather than using explicit solvent molecules, solvent molecules are modeled as dipoles, which vastly simplifies computations and removes the need for an arbitrarily defined dielectric constant. As a result, the system equilibrates over a much shorter time frame during a MD simulation, which enables a large sampling over configurational space in a relatively short time. Each run was 40 ps in length, and coordinates were saved every 1 ps. The standard deviations are obtained from the $\Delta\Delta G$ values computed over the 40-saved coordinate sets. The starting coordinates were all derived from crystal structures.

RESULTS

Crystal Structures of CcPK2M2 and CcPK2M3. The structure of the distal and proximal pockets and the cation-binding loop in CcPK2 is shown in Figure 1. The polypeptide conformation of the cation loop is the same in all peroxidases. CcP, however, lacks the side-chain ligands required for binding either a monovalent or divalent metal ion, and hence, CcP has a water molecule bound in the loop. The His-Asp-Trp hydrogen-bonding arrangement is typical of Class I peroxidases (*22*), which include CcP, APX, and bacterial catalase-peroxidases. The CcPK2 structure, which was engineered to contain the APX cation-binding loop, was used

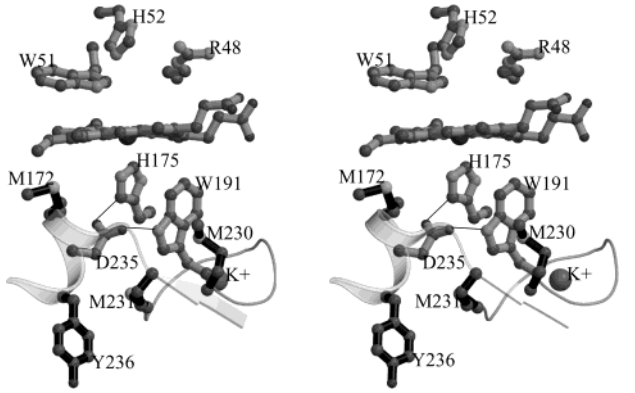

FIGURE 1: Stereoview of the proximal pocket of CcPK2 showing the three Met residues and Tyr236 in relation to key residues in the proximal pocket and the cation loop. Thin lines connecting Asp235 with His175 and Trp191 represent hydrogen bonds.

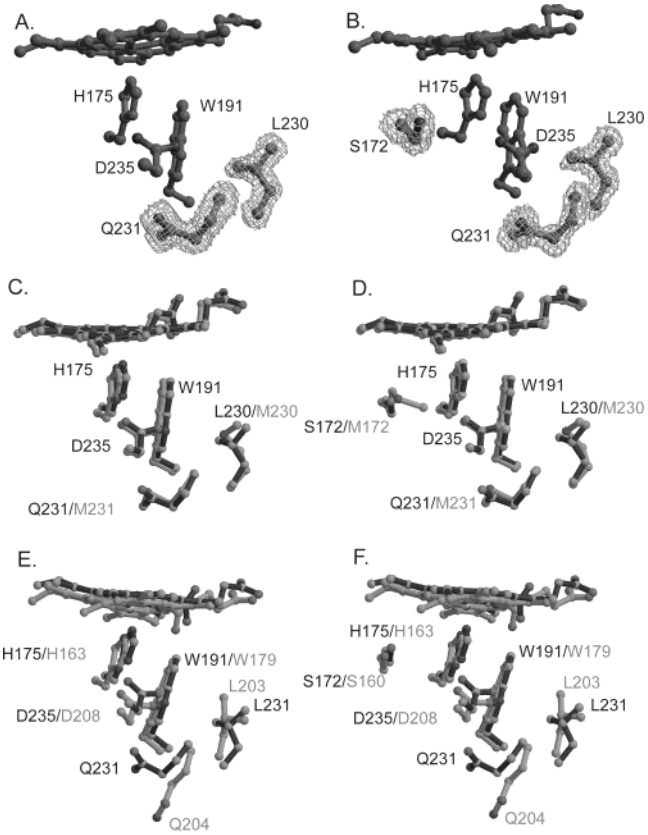

FIGURE 2: Electron density maps for the mutant structures and a comparison between wild-type CcP and APX. (A) $2F_o - F_c$ composite omit map contoured at 1σ around the sites of mutation for CcPK2M2. (B) Same as in A except for the CcPK2M3 mutant. (C) Comparison of CcPK2M2 (black) and wild-type CcP (grey). (D) CcPK2M3 (black) overlaid with wild-type CcP (grey). (E) CcPK2M2 (black) overlaid with wild-type APX (grey) (F) CcPK2M3 (black) overlaid with APX (grey). The figures were generated using Xtalview and Molscript and rendered with Raster 3D (*7*, *33*−*35*).

as the starting model for refinement of both mutants. The mutant side chains were modeled into the difference density calculated from the CcPK2 model. The mutated residues fit well within the density with full occupancy (Figure 2), and the temperature factors of the novel side chains match closely with those of other nearby residues. The final CcPK2M2 model has an R_{factor} of 0.166 and an R_{free} of 0.201 at 1.85 Å, and the final model of CcPK2M3 has an R_{factor} of 0.212 and

Table 2: Steady-State Kinetics of the Reaction between CcP and Yeast Iso-cyt *c*[a]

	10 mM Tris-phosphate at pH 6.0		100 mM Tris-phosphate at pH 6.0	
	k_{cat}	percent activity	k_{cat}	percent activity
wild type	551		5673.4	
CcPK2M2	5.55	1.0	2.80	0.05
CcPK2M3	10.04	1.82	3.22	0.05

[a] Reactions were carried out at pH 6.0 at both low (10 mM) and high (100 mM) ionic strength. In a previous publication (*8*), it was determined that CcPK2 exhibited near wild-type levels of activity at low ionic strength but <1% wild-type activity at high ionic strength.

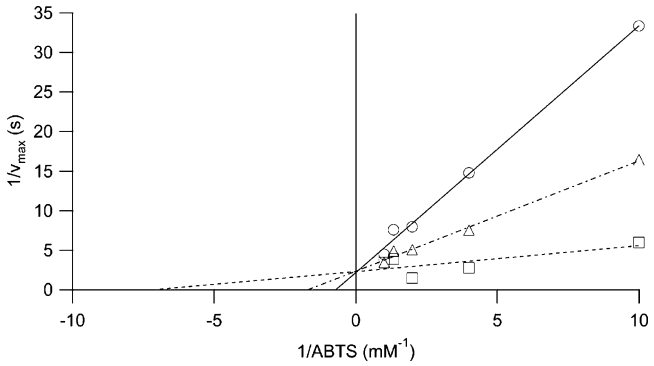

FIGURE 3: ABTS oxidation by wild-type CcP (○), CcPK2M2 (□) and CcPK2M3 (△). All reactions were carried out with a protein concentration of 10 nM. (Wild-type $v_{max} = 2.21$ mM/s and $K_m = 1.4$, CcPK2M2 $v_{max} = 2.33$ mM/s and $K_m = 0.14$, and CcPK2M3 $v_{max} = 2.37$ mM/s and $K_m = 0.59$.)

an R_{free} of 0.235 at 1.82 Å (Table 1). Perturbations of the overall structure caused by the mutations are minimal. The root-mean-square (rms) deviation of backbone atoms between the structure of wild-type CcP and CcPK2M2 is 0.16 and 0.15 Å for CcPK2M3 (Table 1) A superimposition of the CcP mutant structures onto APX is shown in Figure 2. It is apparent that the side chains of L230 and Q231 are positioned as different rotomers than the equivalent residues in APX, while Ser172 overlays nicely with the equivalent Ser160 of APX.

Steady-State Kinetics. As shown previously (*8*), the steady-state activity of CcPK2 with cyt *c* (Fe^{2+}) as the substrate is drastically diminished, maintaining only approximately 10% of the wild-type activity in the absence of potassium. Therefore, it is no surprise that CcPK2M2 and CcPK2M3 also show negligible steady-state activity against cyt *c* (Fe^{2+}). Reactions carried out with yeast cyt *c* (Fe^{2+}) at low ionic strength, 10 mM Tris-phosphate at pH 6.0, in the absence of potassium, showed that these mutants maintained less than 2% of wild-type activity, while reactions carried out at high ionic strength, 100 mM Tris-phosphate at pH 6.0, also in the absence of potassium, showed only 0.05% of wild-type activity (Table 2).

Steady-state activities were also determined for the small molecule peroxidase substrate, ABTS. These experiments show that the mutants oxidize ABTS more efficiently than wild-type CcP (Figure 3). Lineweaver−Burke plots indicate that CcPK2M2 and CcPK2M3 oxidize ABTS with essentially the same maximal velocity as the wild-type but exhibit reduced K_m values. The K_m values are about 10 times lower for CcPK2M2 than for wild-type but only 2.4 times lower for CcPK2M3 than for the wild-type.

Transient-State Kinetics: Compound I Formation. Formation of a porphyrin radical is readily detected in heme peroxidases because oxidation of the porphyrin leads to a large drop in absorbance near the main Soret absorption band. Stopped-flow kinetic studies of compound **I** formation showed that a porphyrin radical does not form in either CcPK2M2 or CcPK2M3. Additionally, the second-order rates of reaction for the mutants are very similar to that of wild-type CcP. The rate of compound **I** formation as a function of peroxide concentration was determined for the CcPK2M2 mutant yielding a second-order reaction rate of 1.6×10^7 M^{-1} s^{-1}. Although data on CcPK2M3 were only collected at one concentration of H_2O_2, the second-order rate of reaction is estimated to be 1.4×10^7 M^{-1} s^{-1}. These values are comparable to that observed for wild-type compound **I** formation, 1.16×10^7 M^{-1} s^{-1}, indicating that the catalytic machinery required for compound **I** formation has not been perturbed by these mutations.

Transient-State Kinetics: Lifetime of the Trp191 Radical. Our previous studies (*7*) indicated that the Trp191 radical can still form in the CcPK2 mutant but that the stability of the Trp191 radical is decreased by K^+ binding in the engineered K^+-binding site. These results were only qualitative, and what has been missing is a more quantitative method for estimating the lifetime of the Trp191 radical. We therefore devised a double-mixing stopped-flow protocol for estimating the stability of the Trp191 radical. In this method, CcP is first converted to compound **I** by mixing with H_2O_2 followed by a variable delay time before mixing with cyt *c* (Fe^{2+}). The shortest delay time that can be measured using this protocol is about 25 ms. Because rapid electron transfer from cyt *c* (Fe^{2+}) to compound **I** requires the presence of the Trp191 radical (*23*), the rate of cyt *c* (Fe^{2+}) oxidation as a function of the delay time can provide an estimate of the Trp191 radical lifetime. We used the Trp191Gly mutant as a negative control, which was unable to oxidize any cyt *c* (Fe^{2+}).

Representative stopped-flow traces are shown in Figure 4. The total amount of cyt *c* (Fe^{2+}) oxidized can be estimated by the total decrease in absorbance at 416 nm. To compare rate constants, we assumed second-order kinetics and the data were fit to the following equation (*18*):

$$\Delta A = l\Delta\epsilon\left(b_o - \frac{\exp[(b_o - a_o)k_1 t] - 1}{\frac{\exp[(b_o - a_o)k_1 t]}{a_o} - \frac{1}{b_o}}\right) \quad (4)$$

where a_o = initial CcP compound **I** concentration, b_o = initial cyt *c* (Fe^{2+}) concentration (this value was fixed), $\Delta\epsilon = -41$ mM^{-1} cm^{-1} (*24*), and l = 1-cm path length. The parameter k_1 corresponds to the following step in the reaction cycle:

$$\text{CcP } (Fe^{4+}\ Trp^{\bullet+}) + \text{cyt } c\ (Fe^{2+}) \xrightarrow{k_1} \text{CcP } (Fe^{4+}\ Trp) + \text{cyt } c\ (Fe^{3+}). \quad (5)$$

For wild-type CcP (Figure 4A), all of the cyt *c* (Fe^{2+}) is oxidized at the same rate from 25-ms to 60-s delay time, which is expected, because the Trp191 radical is very stable. With CcPK2 (Figure 4B), all of the cyt *c* (Fe^{2+}) is oxidized between 25-ms and 60-s delay time, but the rate is much slower, $\sim 2.0 \times 10^6$ M^{-1} s^{-1} after 25-ms delay compared to

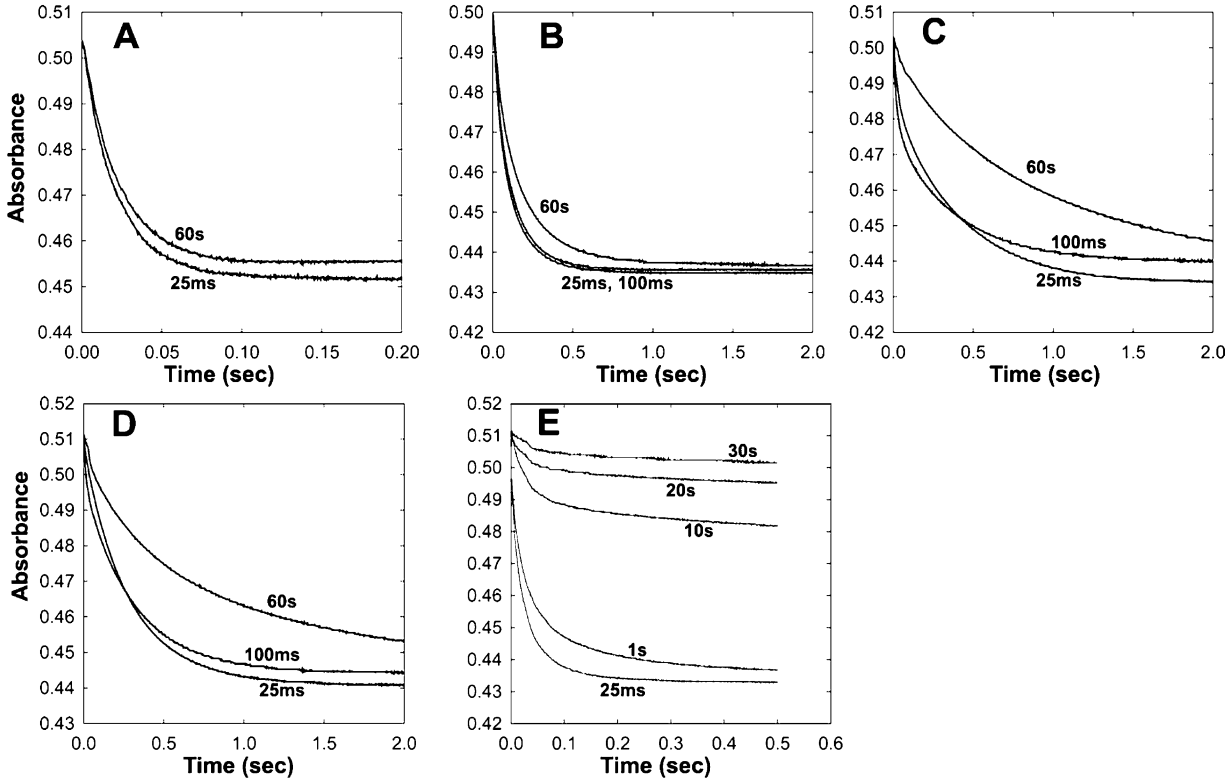

FIGURE 4: Transient-state kinetics of Trp radical oxidation (k_1). Each trace is the average of 3−5 stopped-flow runs. The delay times prior to mixing with cyt *c* (Fe^{2+}) are indicated, (A) wild-type CcP, (B) CcPK2, (C) CcPK2M2, (D) CcPK2M3, (E) CcPK2M3 with Tyr236 converted to Phe. All experiments were performed with a final concentration of less than 3.63 μM CcP compound **I**. The values of k_1 were obtained from a fit of eq 4 with the data from wild-type CcP, CcPK2, CcPK2M2, and CcPK2M3.

14×10^6 M^{-1} s^{-1} for wild-type CcP. With CcPK2M2 and CcPK2M3 (parts C and D of Figure 4), the rates are similar to each other at 25-ms delay time and even slower, $\sim 1.0 \times 10^6$ M^{-1} s^{-1}. Both CcPK2M2 and CcPK2M3 are much more sensitive to the delay time with the rate of cyt *c* (Fe^{2+}) oxidation and total amount of cyt *c* (Fe^{2+}) oxidized decreasing as a function of the delay time.

Perhaps the most informative part of this study is shown in Figure 4E. Here, Tyr236 in CcPK2M3 was converted to Phe. Tyr236 (see Figure 1 for the location of Tyr236) was selected because Tyr236 has been shown to be the site of radical formation in compound **I** in the Trp191Gly mutant (*25*) and hence is the most likely site of radical formation in the absence of a stable Trp191 radical. The most unexpected result is that, at 25-ms delay time, the Y236F mutant oxidizes all of the cyt *c* (Fe^{2+}) at approximately the same rate as wild-type CcP, 20.0×10^6 M^{-1} s^{-1}. It thus appears that changing Tyr236 to Phe in the CcPK2M3 mutant restores the ability of the mutant to oxidize cyt *c* (Fe^{2+}) at the wild-type rate. Note, however, that the Y236F mutant is far more sensitive to the delay time. Both the rate and total amount of cyt *c* (Fe^{2+}) oxidized decreases sharply with delay time and drops close to zero after 10 s. The implications of these results will be considered in the Discussion.

EPR Spectroscopy. The radical of compound **I** in CcP is commonly examined by EPR, which has a very characteristic and easily detectable signal. Previous work on CcPK2 showed that the shape of the compound **I** Trp radical signature, which is in magnetic exchange with the oxyferryl species, did not change but that the intensity of the EPR signal decreased with the addition of potassium. These results indicated that the binding of K^+ was, indeed, destabilizing

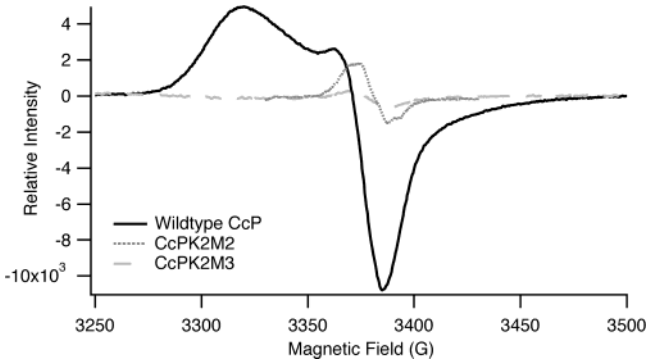

FIGURE 5: EPR spectra of the compound **I** species of the mutants CcPK2M2 and CcPK2M3 in comparison to wild-type CcP. The intensity of the radical signal after approximately 40-s mixing time is greatly reduced in CcPK2M2 and CcPK2M3 in comparison to the intensity of the wild-type spectrum.

the cation Trp191 radical owing to unfavorable electrostatic interactions (*7*). Fishel et al. (*13*) found that changing Met230 and Met231 to Leu resulted in a narrowing of the EPR line shape. The removal of the Met230 and Met231 from the proximal cavity of CcPK2 has a more dramatic effect on the nature of the radical in compound **I** of CcP. The EPR properties of CcPK2M2 and CcPK2M3 reveal two interesting features. First, the maximal intensities of the EPR signals are significantly reduced for CcPK2M2 and CcPK2M3, compared to the wild-type (Figure 5). Second, and perhaps most notably, the line shape of the mutant spectra is more characteristic of an isolated tyrosine radical, such as the one seen in mutants of *Proteus mirabilis* catalase and in a mutant of horseradish peroxidase with Phe172 replaced by Tyr (*26*, *27*). Data were collected on samples both in the presence

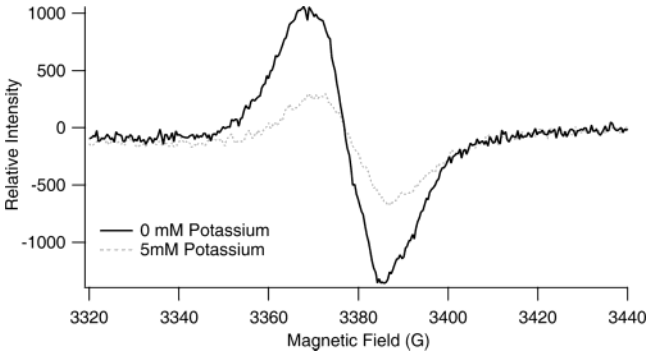

FIGURE 6: EPR spectra of compound **I** in CcPK2M3 in the presence and absence of 5 mM potassium. CcPK2M3 exhibits a reduction in signal intensity in the presence of potassium, indicating that potassium binding in the cation-binding loop, K2, does significantly destabilize the radical. The spectral trace closely resembles that of a tyrosinyl radical.

Table 3: Data from the Polaris Calculations on the $\Delta\Delta G$ of Solvation of the Trp Radical in CcP, APX, CcPK2, CcPK2M2, and CcPK2M3[a]

protein	K^+ charge	$\Delta\Delta G$ (kcal/mol)
wild-type CcP		-4.92 ± 1.07
wild-type APX	on	-2.65 ± 0.75
wild-type APX	off	-3.17 ± 0.6
CcPK2	on	-4.11 ± 0.79
CcPK2	off	-4.64 ± 0.80
CcPK2M2	on	-3.71 ± 0.92
CcPK2M3	on	-2.44 ± 0.83

[a] The charge on the K^+ ion was turned on or off by setting the charge of the K^+ ion to +1 and the Asp ligand to −1 or by setting both charges to 0. The data indicate that the mutations lead to the decrease in stability of the Trp cation radical. Note that CcPK2M3 has essentially the same $\Delta\Delta G$ of solvation of the Trp radical as APX.

and absence of potassium, and it is clear that, while potassium does have an effect on the stability of the radical species, this effect is not nearly as dramatic as the effect of the mutations themselves (Figure 6). The CcPK2M2 mutant where Tyr236 is converted to Phe is EPR-silent with very little trace of any radical indicating that Tyr236 may be the primary site of radical formation in the absence of a stable Trp191 radical (data not shown).

Electrostatic Calculations. It is well-known that changing Trp191 to Gly introduces a cavity that can bind positively charged compounds, indicating that the Trp191 pocket is designed to stabilize a cation (*28*, *29*). Electrostatic calculations have been used to provide a more quantitative understanding of the differences in the ability of CcP and APX to stabilize the Trp cation radical (*5*, *7*, *11*). The Polaris method previously used by Jensen et al. (*11*) provides an estimate for the electrostatic $\Delta\Delta G$ of transfer of the Trp191 cation radical from water to protein. Table 3 shows the results of a series of similar Polaris calculations carried out on wild-type CcP and APX in addition to the mutants used in this study. As noted earlier by Jensen et al. (*11*), the Trp191 cation radical is more stable in wild-type CCP than in APX. Eliminating the positive charge on K^+ in APX increases the stability of the Trp191 cation from −2.65 to −3.15 kcal/mol, while introducing the cation site in CcP (CcPK2 in Table 3) decreases the Trp191 cation stability from −4.92 to −4.11 kcal/mol. Therefore, the engineered cation site alone in CcPK2 is not sufficient to decrease the stability of the Trp191 cation radical to −2.65 kcal/mol computed for APX. However, when the K^+ site is introduced into CcP and when Met230 and Met231 are converted to the corresponding residues in APX (CcPK2M2 in Table 3), the stability drops to −3.71 kcal/mol. Changing the third Met, Met172, to Ser further lowers the stability of the Trp191 cation radical to −2.44 kcal/mol, which is very close to −2.65 kcal/mol computed for APX. These results indicate that both the three-proximal-side Met residues and the K^+ site are important for controlling the electrostatic stability of the Trp191 cation radical.

DISCUSSION

While it is clear from earlier work (*7*, *8*) that introducing a K^+-binding site into CcP leads to the K^+-dependent destabilization of the Trp cation radical, our present study illustrates that metal binding accounts for only part of the difference in the location and stability of the compound **I** radical. Similar conclusions were reached by Jensen et al. using purely computational methods (*11*). The EPR spectrum of CcPK2 (*7*, *8*) is similar to the characteristic Trp191 radical of wild-type CcP but with a greatly diminished intensity. Changing even two of the three Met residues in the proximal pocket of CcPK2 to the corresponding residues in APX eliminates the Trp191 EPR signal and generates a Tyr-like EPR signal. Integration of the EPR data for CcPK2M2 indicates that the Tyr radical exhibits about a 14% spin equivalent if we assume the wild type gives 100%. If only 14% of the oxidizing equivalents are available as a free radical in the mutants, then the question arises as to how all of the cyt *c* (Fe^{2+}) can be oxidized. In the double-mixing stopped-flow experiments, CcP was in 3-fold excess over cyt *c*, which was necessary to ensure that reduction of Fe^{IV}−O is minimized. As a result, substoichiometric CcP-oxidizing equivalents are required to oxidize all of the cyt *c*. Another source of the apparent paradox is that the kinetic experiments are at protein concentrations near 7 μM, while the EPR experiments required at least 150 μM and on the order of 40−60 s to add peroxide and freeze the sample for EPR studies. The spontaneous decay of compound **I** is known to lead to intermolecular cross-linking through Tyr residues (*30*), which increases at higher protein concentrations. Cross-linking is also a more facile process in mutants with an unstable radical (*31*). Therefore, we suspect that the radical site(s) more readily decays at EPR-level protein concentrations, and hence, the spin equivalents estimated from the EPR spectra are likely to be an underestimate of the radical site(s) available for oxidization of cyt *c* (Fe^{2+}) in the kinetic experiments.

The most likely radical site in the Met mutants is Tyr236 because changing Tyr236 to Phe in CcPK2M2 results in a protein that is EPR-silent (data not shown). Thus, the EPR data indicate that the rank order of Trp191 radical stability is CcP > CcPK2 > CcPK2M2 ∼ CcPK2M3 > CcPK2M3 Y236F. This is the same order based on the data in Figure 4, where the rate and extent of cyt *c* (Fe^{2+}) oxidation as a function of delay time are compared.

The data in Figure 4 are complicated by the fact that changing Tyr236 to Phe in the CcPK2M3 mutant actually increases the rate of cyt *c* (Fe^{2+}) oxidation at 25-ms delay to that of wild-type CcP, yet the extent of cyt *c* (Fe^{2+}) oxidation drops to nearly zero within 10-s delay time. The

model that we favor to help us understand these results assumes the following equilibration is present in compound **I**.

$$\underset{\text{Active}}{Trp^{\bullet+}} + Tyr \rightleftarrows \underset{\text{Inactive}}{Trp} + Tyr^{\bullet} \quad (6)$$

Musah and Goodin (*25*) showed that Tyr236 forms a radical in the Trp191Gly mutant and thus provides a secondary site of oxidation. In wild-type CcP, the above equilibrium favors $Trp^{\bullet+}$. However, in CcPK2, the equilibrium shifts to $Tyr^{\bullet}$. The amount can be estimated by comparing the rate of cyt *c* (Fe^{2+}) oxidation computed from the data in Figure 4. For CcPK2, the rate is about 15% that of the wild-type, which indicates that, after 25-ms delay time, $Trp^{\bullet+}$ accounts for 15% of the oxidizing equivalent. Before cyt *c* (Fe^{2+}) can reduce $Trp^{\bullet+}$ to Trp, Trp191 must be reoxidized by Tyr236 to maintain the Trp191/Tyr236 equilibrium, which explains why all of the cyt *c* (Fe^{2+}) can be oxidized. This process is relatively insensitive to the delay time up to the longest delay time measured, 120 s (data not shown). With CcPK2M2 and CcPK2M3, only ~6.0% of the oxidizing equivalent remains on Trp191 after 25-ms delay time and both the rate and extent of cyt *c* (Fe^{2+}) oxidation drops off as a function of the delay time, indicating that the Trp191/Tyr236 equilibrium is not stable and that Tyr236 is able to oxidize other sites besides Trp191.

The data in Figure 4E provide the key to understanding the role of Tyr236. The rate of cyt *c* (Fe^{2+}) oxidation increases to the wild-type rate when Tyr236 is changed to Phe in the CcPK2M3 mutant because there is no other stable site for equilibration of the Trp191 radical since the Tyr236 has been removed. In effect, the $Trp^{\bullet+}$ is still very unstable but has fallen into a kinetic trap and has no other site with which to equilibrate. As a result, at the very shortest delay time that we can measure, 25 ms, there is a full spin equivalent remaining on Trp191, and hence, the rate of cyt *c* (Fe^{2+}) oxidation is the same as the wild type. However, with time, the Trp191 radical irreversibly migrates to other sites, most likely one of the other 13 Tyr residues in CcP. Two factors may be related to why Tyr236 is the favored site for equilibration with the Trp191 radical. First, Tyr236 contacts two other Trp residues thus forming an aromatic cluster that might provide some stabilization of a Tyr radical. Second, Tyr236 immediately follows Asp235, which hydrogen bonds with Trp191 (Figure 1). Thus, there is a short hydrogen bond/σ-bonded connection between Trp191 and Tyr236, which could provide a facile path for electron transfer.

An important part of this study was to explore how well computational approaches designed to determine the electrostatic stabilization of the Trp191 cation radical correlate with experiments. There is a remarkably good agreement between the Polaris calculations and the experimental results. The order of the calculated electrostatic stabilization of the Trp191 cation radical is CcP > CcPK2 > CcPK2M2 > CcPK2M3 ~ APX. This is the same order as the steady-state activity, the rate of cyt *c* (Fe^{2+}) oxidization using the single-turnover method described in Figure 4, and EPR, although the activity profiles of CcPK2M2 and CcPK2M3 are very similar. Most interestingly, CcPK2M3 has nearly the same $\Delta\Delta G$ of stabilization as APX, −2.44 kcal/mol, for CcPK2M3, compared to −2.65 kcal/mol for APX. Therefore, as noted earlier by Fishel et al. (*13*), the Met residues in CcP are important in the electrostatic stabilization of the Trp191 cation radical. Moreover, the lack of these Met residues and the presence of the K^+ site prevent formation of a stable cation Trp radical in APX. Relevant to the role of Met residues in CcP compound **I** is the recent 1.3-Å structure of CcP compound **I** compared to the 1.2-Å structure of resting state CcP (*32*). In the resting state, Met172 and a surface loop centered on residue 194 occupy two positions. Both regions are fixed in place in compound **I** to help stabilize the Trp191 radical. The single conformation of Met172 in compound **I** directly contacts the heme ligand, His175, which, in turn, directly contacts the Trp191 indole ring. Therefore, Met172 moves closer to Trp191 to help stabilize the extra positive charge on the Trp191 cation radical.

We had anticipated that the inability to form a Trp191 radical in the mutants might lead to formation of a porphyrin radical. However, the stopped-flow work shows that a porphyrin radical still does not form in any of the mutants. As we discussed earlier, this is because Tyr236 provides the next most stable oxidation site. However, changing Tyr236 to Phe still does not enable a porphyrin radical to form. As the data in Figure 4E indicate, changing Tyr236 to Phe in CcPK2M3 enables a transient Trp191 radical to form but the oxidizing equivalent rapidly migrates to other site(s), one of which is not the porphyrin. Such promiscuous movement of the radical among other sites, most likely, other Tyr residues, can also help to rationalize the increased activity toward ABTS. The decrease in the K_m value for the mutants can be explained by the increased population of surface radicals providing a higher probability of a favorable interaction occurring between the enzyme and small molecule substrates.

Finally, we note the remaining areas that require further exploration. We now have learned how to "turn off" the Trp191 radical in CcP, and the excellent correlation between EPR, steady-state activity, stopped-flow data, and the Polaris calculations clearly demonstrates that electrostatic stabilization is the key to stabilization of the Trp191 cation radical. The next step is to carry out the inverse experiment and "turn on" the Trp radical in APX. Given the success with CcP, it should be possible to introduce the three key Met residues into the proximal pocket of APX thus enabling the stabilization of the Trp179 radical. A more complex problem is to determine if the porphyrin is the default site of oxidation if there are no other more favorable sites, i.e., Trp or Tyr. Alternatively, there could be additional unknown factors that favor porphyrin oxidation as opposed to oxidation of Tyr or Trp residues. Addressing this problem will require a combination of mutagenic, spectroscopic, and computational approaches that will likely be more complicated to interpret owing to the greater complexity in both size and electronic structure of the heme compared to aromatic side chains.

ACKNOWLEDGMENT

We thank Dr. Angel J. Di Bilio of the California Institute of Technology, Pasadena, CA for his expert advice on the collection and preliminary analysis of EPR data.

REFERENCES

1. Stubbe, J., and van der Donk, W. A. (1998) Protein radicals in enzyme catalysis, *Chem. Rev. 98*, 705−762.
2. Sivaraja, M., Goodin, D. B., Smith, M., and Hoffman, B. M. (1989) Identification by ENDOR of Trp191 as the free-radical site in cytochrome *c* peroxidase compound ES, *Science 245*, 738−740.
3. Erman, J. E., and Yonetani, T. (1975) A kinetic study of the endogenous reduction of the oxidized sites in the primary cytochrome *c* peroxidase-hydrogen peroxide compound, *Biochim. Biophys. Acta 393*, 350−357.
4. Dolphin, D., Forman, A., Borg, D. C., Fajer, J., and Felton, R. H. (1971) Compounds I of catalase and horseradish peroxidase: π-cation radicals, *Proc. Natl. Acad. Sci. U.S.A. 68*, 614−618.
5. Pappa, H., Patterson, W. H., and Poulos, T. L. (1996) The homologous tryptophan critical for cytochrome *c* peroxidase function is not essential for ascorbate peroxidase activity, *J. Biol. Inorg. Chem. 1*, 66−66.
6. Patterson, W. R., and Poulos, T. L. (1995) Crystal structure of recombinant pea cytosolic ascorbate peroxidase, *Biochemistry 34*, 4331−4341.
7. Bonagura, C. A., Sundaramoorthy, M., Pappa, H. S., Patterson, W. R., and Poulos, T. L. (1996) An engineered cation site in cytochrome *c* peroxidase alters the reactivity of the redox active tryptophan, *Biochemistry 35*, 6107−6115.
8. Bonagura, C. A., Sundaramoorthy, M., Bhaskar, B., and Poulos, T. L. (1999) The effects of an engineered cation site on the structure, activity, and EPR properties of cytochrome *c* peroxidase, *Biochemistry 38*, 5528−5545.
9. Mittler, R., and Zilinskas, B. A. (1991) Molecular cloning and nucleotide sequence analysis of a cDNA encoding pea cytostolic cscorbate peroxidase, *FEBS Lett. 289*, 257−259.
10. Patterson, W. R., Poulos, T. L., and Goodin, D. B. (1995) Identification of a porphyrin π cation radical in ascorbate peroxidase compound I, *Biochemistry 34*, 4342−4345.
11. Jensen, G. M., Bunte, S. W., Warshel, A., and Goodin, D. B. (1998) Energetics of cation radical formation at the proximal active site tryptophan of cytochrome *c* peroxidase and ascorbate peroxidase, *J. Phys. Chem. B 102*, 8221−8228.
12. Liu, R. Q., Miller, M. A., Han, G. W., Hahm, S., Geren, L., Hibdon, S., Kraut, J., Durham, B., and Millet, F. (1994) Role of methionine 230 in intramolecular electron transfer between the oxyferryl heme and tryptophan 191 in cytochrome *c* peroxidase compound II, *Biochemistry 33*, 8678−8685.
13. Fishel, L. A., Farnum, M. F., Mauro, M., Miller, M. A., Kraut, J., Liu, Y. L., and Scholes, C. P. (1991) Compound I radical in site-directed mutants of cytochrome *c* peroxidase as probed by electron paramagentic resonance and electron−nuclear double resonance, *Biochemistry 30*, 1986−1996.
14. Ho, S. N., Hunt, H. D., Horton, R. M., Pullen, J. K., and Pease, L. R. (1989) Site-directed mutagenesis by overlap extension using the polymerase chain reaction, *Gene 77*, 51−59.
15. Fishel, L. A., Villafranca, J. E., Mauro, J. M., and Kraut, J. (1987) Yeast cytochrome *c* peroxidase: Mutagenesis and expression in *Escherichia coli* show tryptophan-51 is not the radical site in compound I, *Biochemistry 27*, 351−360.
16. Iffland, A., Gendreizig, S., Tafelmeyer, P., and Johnsson, K. (2001) Changing the substrate specificity of cytochrome *c* peroxidase using directed evolution, *Biochem. Biophys. Res. Commun. 286*, 126−132.
17. Bhaskar, B., Bonagura, C. A., Li, H., and Poulos, T. L. (2002) Cation-induced stabilization of the engineered cation-binding loop in cytochrome *c* peroxidase (CcP), *Biochemistry 41*, 2684−2693.
18. Hahm, S., Miller, M. A., Geren, L., Kraut, J., Durham, B., and Millett, F. (1994) Reaction of horse cytochrome *c* with the radical and the oxyferryl heme in cytochrome *c* peroxidase compound I, *Biochemistry 33*, 1463−1480.
19. Otwinowski, Z., and Minor, W. (1997) Processing of X-ray diffraction data collected in oscillation mode, *Methods Enzymol. 276*, 307−326.
20. Brunger, A. T., Adams, P. D., Clore, G. M., DeLano, W. L., Gros, P., Grosse-Kunstleve, R. W., Jiang, J.-S., Kuszewski, J., Nilges, M., Pannu, N. S., Read, R. J., Rice, L. M., Simonson, T., and Warren, G. L. (1998) Crystallography & NMR System: A new software suite for macromolecular structure determination, *Acta Crystallogr., Sect. D 54*, 905−921.
21. Warshel, A., and Florian, J. (1998) Computer simulations of enzyme catalysis: Finding out what has been optimized by evolution, *Proc. Natl. Acad. Sci. U.S.A. 95*, 5950−5955.
22. Welinder, K. G. (1992) Superfamily of plant, fungal, and bacterial peroxidases, *Curr. Biol. 2*, 388−393.
23. Mauro, J. M., Fishel, L. A., Hazzard, J. T., Meyer, T. E., Tollin, G., Cusanovich, M. A., and Kraut, J. (1987) Tryptophan-191 → phenylalanine, a proximal-side mutation in yeast cytochrome *c* peroxidase that strongly affects the kinetics of ferrocytochrome *c* oxidation, *Biochemistry 27*, 6243−6256.
24. Margoliash, E., and Frohwirt, N. (1959) Spectrum of horse-heart cytochrome *c*, *Biochem. J. 71*, 570−572.
25. Musah, R. A., and Goodin, D. B. (1997) Introduction of novel substrate oxidation into cytochrome *c* peroxidase by cavity complementation: Oxidation of 2-aminothiazole and covalent modification of the enzyme, *Biochemistry 36*, 11665−11674.
26. Miller, V. P., Goodin, D. B., Friedman, A. E., Hartmann, C., and Ortiz de Montellano, P. R. (1995) Horseradish peroxidase Phe172 → Tyr mutant. Sequential formation of compound I with a porphyrin radical cation and a protein radical, *J. Biol. Chem. 270*, 18413−18419.
27. Andreoletti, P., Gambarelli, S., Sainz, G., Stojanoff, V., White, C., Desfonds, G., Gagnon, J., Gaillard, J., and Jouve, H. M. (2001) Formation of a tyrosyl radical intermediate in *Proteus mirabilis* catalase by directed mutagenesis and consequences for nucleotide reactivity, *Biochemistry 40*, 13734−13743.
28. Miller, M. A., Han, G. W., and Kraut, J. (1994) A cation binding motif stabilizes the compound I radical of cytochrome *c* peroxidase, *Proc. Natl. Acad. Sci. U.S.A. 91*, 11118−11122.
29. Miller, M. A., Liu, R. Q., Hahm, S., Geren, L., Hibdon, S., Kraut, J., Durham, B., and Millett, F. (1994) Interaction domain for the reaction of cytochrome *c* with the radical and the oxyferryl heme in cytochrome *c* peroxidase compound I, *Biochemistry 33*, 8686−8693.
30. Spangler, B. D., and Erman, J. E. (1986) Cytochrome *c* peroxidase compound I: Formation of covalent protein crosslinks during the endogenous reduction of the active site, *Biochim. Biophys. Acta 872*, 155−157.
31. Pfister, T. D., Gengenbach, A. J., Syn, S., and Lu, Y. (2001) The role of redox-active amino acids on compound I stability, substrate oxidation, and protein cross-linking in yeast cytochrome *c* peroxidase, *Biochemistry 40*, 14942−14951.
32. Bonagura, C. A., Bhaskar, B., Shimizu, H., Li, H., Sundaramoorthy, M., McRee, D. E., Goodin, D. B., and Poulos, T. L. (2003) High-resolution crystal structures and spectroscopy of native and compound I cytochrome *c* peroxidase, *Biochemistry 42*, 5600−5608.
33. Kraulis, P. J. (1991) Molscript: A program to produce both detailed and schematic plots of protein structures, *J. Appl. Crystalogr. 24*, 946−950.
34. Merrit, E. A. B., D. J. (1997) Raster3D: Photorealistic molecular graphics, *Methods Enzymol. 277*, 505−524.
35. McRee, D. E. (1999) XtalView/Xfit—A Versatile Program for Manipulating Atomic Coordinates and Electron Density, *J. Struct. Biol. 125*, 156−165.

BI049531G